Study of the Reaction $K^+n \to K^+N^{*0}$ at 12 GeV/c†

D. Lissauer,* A. Firestone,‡ J. Ginestet,§ G. Goldhaber, ‖ and G. H. Trilling

Department of Physics and Lawrence Berkeley Laboratory, University of California, Berkeley, California 94720

(Received 12 May 1972)

We have studied the reaction $K^+n \to K^+N^{*0} \to K^+\pi^-p$ at 12 GeV/c using data obtained in an exposure of the deuterium-filled SLAC 82-in. bubble chamber to an rf-separated K^+ beam. The $M(p\pi^-)$ spectrum exhibits a very large enhancement below 1.8 GeV which we identify as primarily a diffractive effect. A partial-wave analysis of this enhancement shows that the data can be interpreted in terms of $P_{1/2}$, $D_{3/2}$, and $F_{5/2}$ contributions. The $P_{1/2}$ contribution which dominates at very low momentum transfers appears to peak around 1.25 GeV. If this state is associated with the Roper resonance, a mechanism which produces a downward mass shift of about 200 MeV for the diffractively produced $p\pi^-$ decay mode is implied.

I. INTRODUCTION

In this paper we report the results of our study of the reaction

$$K^+n \to K^+N^{*0} \to K^+\pi^-p \tag{1}$$

at 12-GeV/c incident momentum. The symbol N^* in (1) is intended to denote all structure observed in the $p\pi^-$ system whether or not it conforms to the established baryon resonances.

The data on which our analysis is based were obtained in a 500 000-photograph exposure of the SLAC 82-in. bubble chamber, filled with deuterium, to a 12-GeV/c rf-separated K^+ beam. Reaction (1) involves the same topologies (namely four-prong events with at least one stopping track and three-prong events) as those used in a study of coherent Q^+ production in deuterium based on the same film. Complete details of the data handling are given in our report of that work.[1] A total of 6784 events are kinematically consistent with the reaction $K^+d \to K^+\pi^-pp$ with a χ^2 probability greater than 0.1%. Of these, 40% have two visible protons and 60% have only one visible proton in the bubble chamber. Motivated by the impulse approximation, we assume the slower proton in the laboratory to be the spectator nucleon and the faster proton to be the recoiling particle. With this selection, the slower proton has an observed momentum spectrum in fair agreement with that expected from the Hulthén wave function. The distribution of the angle between the beam and the spectator is isotropic as expected. Events with spectator momenta greater than 300 MeV/c were excluded from the subsequent analysis, leaving a sample of 6454 events, which correspond to a cross section of 400 ± 20 μb.[2]

II. GENERAL FEATURES

Figure 1 shows the Dalitz plot for the reaction $K^+n \to K^+\pi^-p$. Its prominent features include a strong low-mass enhancement in the $p\pi^-$ system, $K^*(890)$ and $K^*(1420)$ bands, and a wide band at $M^2(K\pi) \approx 3$ GeV². There are relatively few events in the region of the Dalitz plot external to these structures. The details of the $K^+\pi^-$ structure have been discussed elsewhere and will not be considered further here.[3] Figure 2 shows the $p\pi^-$ mass spectrum; its major feature is a large, broad mass enhancement centered near $M(p\pi) \approx 1.4$ GeV which drops off sharply at $M(p\pi) \approx 1.8$ GeV. Figure 3 shows the Chew-Low plot, relating t, the square of the momentum transfer between the incoming and outgoing K^+ mesons, with $M^2(p\pi)$. The low $M(p\pi)$ enhancement is produced peripherally although it does extend to fairly high t $[\gtrsim 1$ (GeV/c)²$]$.

We now consider in a more detailed way the features of the $p\pi^-$ mass enhancement. In this discussion and in all subsequent analysis, no attempt was made to remove K^* events within the $p\pi^-$ mass bands under study. Indeed, because of duality, it is difficult to know what fraction, if any, of these K^* events should be regarded as not contributing simultaneously to the N^* band. The actual magnitudes of the K^* contributions in the region $M(p\pi)$ < 1.8 GeV, in three momentum-transfer intervals used in our later analysis, can be seen in the $K\pi$ mass spectra shown in Fig. 4.

Figure 5 shows the differential cross section $d\sigma/dt'$ for $M(p\pi)$ below 1.8 GeV, where $t' = |t - t_{min}|$ and t_{min} is the kinematic lower limit for t. The distribution evidently cannot be represented by a single exponential linear in t', but can be adequately fitted by the sum of two exponentials,

$$\frac{d\sigma}{dt'} = A_1 e^{-b_1 t'} + A_2 e^{-b_2 t'}, \tag{2}$$
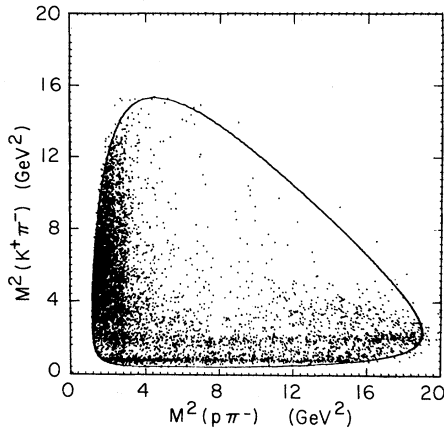
FIG. 1. Dalitz plot for reaction $K^+n \to K^+\pi^-p$.

in which

$$A_1 = 1120 \pm 70 \ \mu b/(\text{GeV}/c)^2,$$

$$A_2 = 470 \pm 30 \ \mu b/(\text{GeV}/c)^2,$$

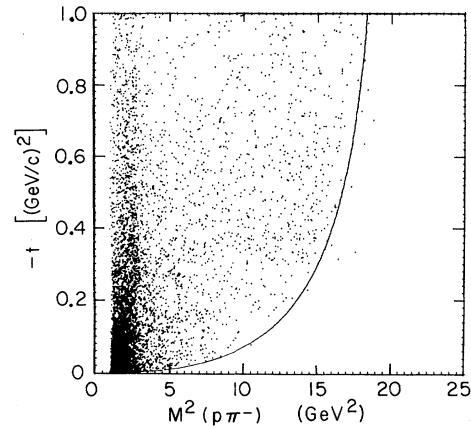$$b_1 = 17 \pm 2 \ (\text{GeV}/c)^{-2},$$

$$b_2 = 4 \pm 1 \ (\text{GeV}/c)^{-2}.$$

Figure 6 shows the differential cross sections $d\sigma/dt'$ in the following 0.2-GeV bins of $M(p\pi)$: (a) $1.1 < M(p\pi) < 1.3$ GeV, (b) $1.3 < M(p\pi) < 1.5$ GeV, (c) $1.5 < M(p\pi) < 1.7$ GeV. The break in the slopes of $d\sigma/dt'$ at $t' \approx 0.2$ $(\text{GeV}/c)^2$ is most marked in the lowest $M(p\pi)$ bin and disappears at the highest bin. The distributions $d\sigma/dt'$ can be fitted to a single linear exponential in the low-t' region,

$$\frac{d\sigma}{dt'} = Ae^{-bt'} \text{ for } t' < 0.2 \ (\text{GeV}/c)^2 \qquad (3)$$

with the results $b = 14 \pm 2$, 8 ± 1.5, and 3.5 ± 1 (GeV/c)$^{-2}$ in the three $M(p\pi)$ bins (a), (b), and (c), respectively.

Our observations based on reaction (1) are very
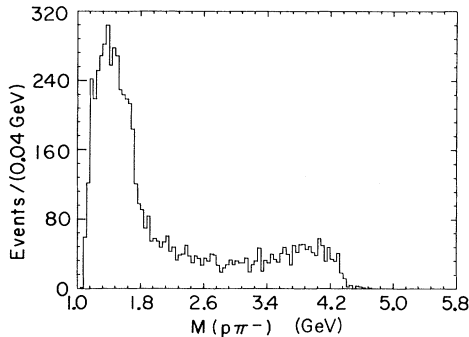
FIG. 2. $M(p\pi^-)$ distribution for all $K^+n \to K^+\pi^-p$ events.

similar to those of Boesebeck et al.[4] based on the reactions $\pi^+p \to \pi^+\pi^0p$ and $\pi^+p \to \pi^+\pi^+n$. Thus the $M(p\pi)$ enhancement shown in Fig. 2 agrees in both position and width with their $I = \frac{1}{2}$ $N\pi$ structure, and the shape and dependence on $p\pi$ mass of our $d\sigma/dt'$ distributions are similar to theirs. Furthermore,

FIG. 3. Chew-Low plot $M^2(p\pi^-)$ vs $-t$ for $K^+n \to K^+\pi^-p$.
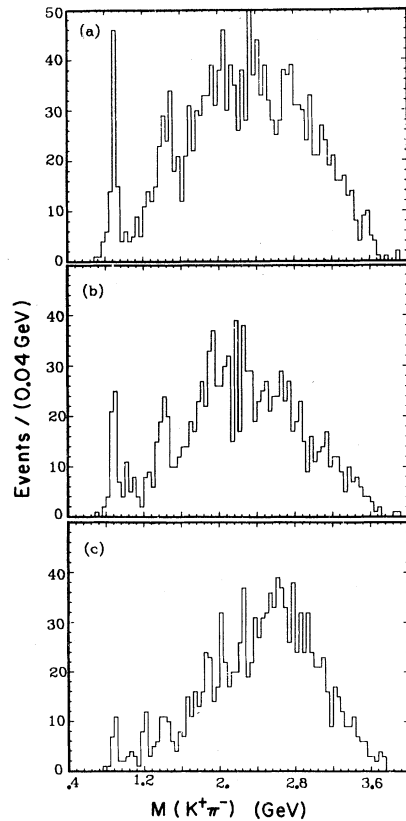
FIG. 4. $M(K^+\pi^-)$ distribution for events in the low-mass $p\pi^-$ enhancement, $M(p\pi^-) < 1.8$ GeV in three ranges of momentum transfer, (a) $t' < 0.1$ (GeV/c)^2, (b) $0.1 < t' < 0.3$ (GeV/c)^2, (c) $t' > 0.3$ (GeV/c)^2.
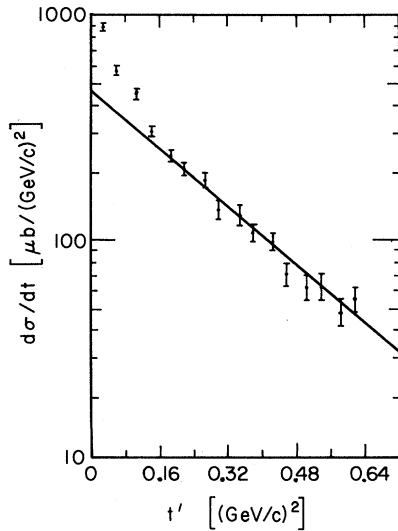
FIG. 5. $d\sigma/dt$ vs t' for $K^+n \to K^+\pi^-p$ events such that $M(p\pi^-) < 1.8$ GeV. The curve corresponds to an exponential with slope equal to 4 $(\text{GeV}/c)^{-2}$.

similarly shaped $M(p\pi)$ enhancements have been reported for the reactions $pn \to pp\pi^-$ and $nC \to p\pi^-C$, where C represents a carbon nucleus.[5,6]

The complexity of the production angular distribution [see Eq. (2)] suggests that there may be more than one mechanism responsible for the production of the entire $M(p\pi)$ enhancement. Figures 7(a)–7(c) show the $p\pi^-$ mass spectra for the three

following regions of t': (i) $t' < 0.1$ $(\text{GeV}/c)^2$, (ii) $0.1 < t' < 0.3$ $(\text{GeV}/c)^2$, (iii) $t' > 0.3$ $(\text{GeV}/c)^2$. It is clear from Fig. 7 that in the very-low-momentum-transfer region, the mass spectrum is shifted toward lower masses than is the case at higher momentum transfers. At the highest-t' region, there are indications of structure near 1.5 and 1.7 GeV.

As seen in Fig. 7(a), the mass enhancement at $t' < 0.1$ $(\text{GeV}/c)^2$ is peaked at $M(p\pi) \approx 1.28$ GeV. Since a potential contributor to this peak is the process $K^+n \to K^+\Delta^0(1236)$, we have determined the number of Δ^0 events expected from the known $K^+p \to K^0\Delta^{++}$ cross section.[7] This number is 35, from which it follows that the Δ^0 contribution to any one bin of Fig. 7(a) is less than 10%. Thus the observed peak is *not* associated with the $I = \frac{3}{2}$ $N\pi$ state; i.e., its isospin is principally $\frac{1}{2}$.

We have also examined the distribution of $M(p\pi^0)$ from the charge exchange reaction $K^+n \to K^0\pi^0p$ observed in our film. The identification of this reaction is difficult because of contamination by processes with two or more π^0 in the final state. A carefully selected sample shows a clear Δ^+ signal centered at $M \approx 1240$ MeV whose population is in agreement with the number expected on the basis of the $K^0\Delta^{++}$ cross section. In the $K^0\pi^0p$ reaction we find no $p\pi^0$ enhancement other than what is accounted for by Δ^+ production. This implies that the $I = \frac{1}{2}$ $N\pi$ enhancement observed in reaction (1)
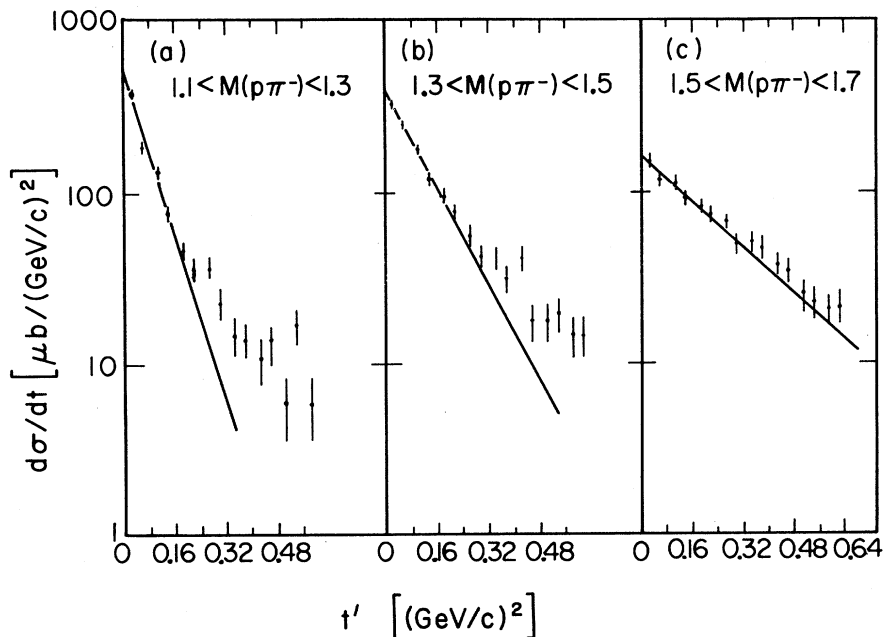

FIG. 6. $d\sigma/dt$ vs t' for three ranges of $M(p\pi^-)$, (a) $1.1 < M(p\pi^-) < 1.3$ GeV, (b) $1.3 < M(p\pi^-) < 1.5$ GeV, (c) $1.5 < M(p\pi^-) < 1.7$ GeV. The curves correspond to exponentials with slopes equal to 14, 8, and 3.5 $(\text{GeV}/c)^{-2}$ for parts (a), (b), and (c), respectively.
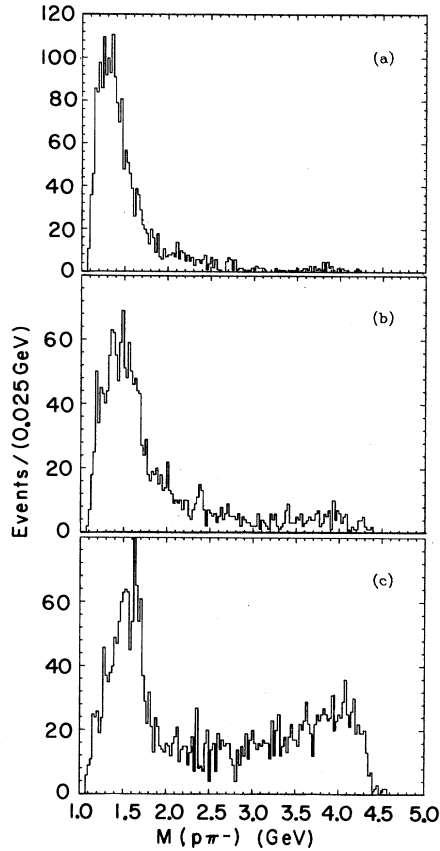
FIG. 7. $M(p\pi^-)$ spectra for three t' intervals, (a) $t' < 0.1$ $(\text{GeV}/c)^2$, (b) $0.1 < t' < 0.3$ $(\text{GeV}/c)^2$, (c) $t' > 0.3$ $(\text{GeV}/c)^2$.

is produced almost exclusively by isoscalar exchange and hence is most naturally interpreted as diffractive dissociation of the incident nucleon. As already noted by Boesebeck et al.,[4] the central value of the diffractive enhancement falls considerably lower than for any of the N^* resonances established in phase shift analysis.

Although the above discussion was focused on the momentum transfer region $t' < 0.1$ $(\text{GeV}/c)^2$, similar arguments apply to the higher-momentum-transfer data leading to the conclusion that the low-mass enhancements in Figs. 7(b) and 7(c) are also in the $I = \frac{1}{2}$ $N\pi$ system produced in diffractive dissociation.

To study the decay characteristics of the $p\pi^-$ enhancement, we have calculated as a function of $M(p\pi)$ the mean values of the spherical harmonics Y_l^m in the Gottfried-Jackson frame for the three t' regions (i), (ii), (iii) defined above. The angle θ is taken between the incident neutron and the outgoing proton in the $p\pi$ rest system. The $\langle Y_l^0 \rangle$ for $1 \leq l \leq 6$ are shown in Figs. 8, 9, and 10 for the three t' regions. Numerical values of the moments up to $l = 4$ and populations for $M(p\pi) < 1.8$ GeV are
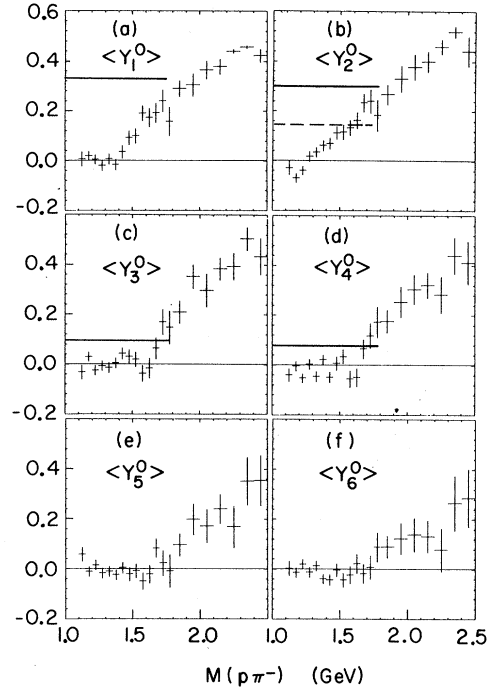
FIG. 8. Values of $\langle Y_l^0 \rangle$ as a function of $M(p\pi^-)$ in the range $t' < 0.1$ $(\text{GeV}/c)^2$. The horizontal lines indicate upper limits discussed in the text.
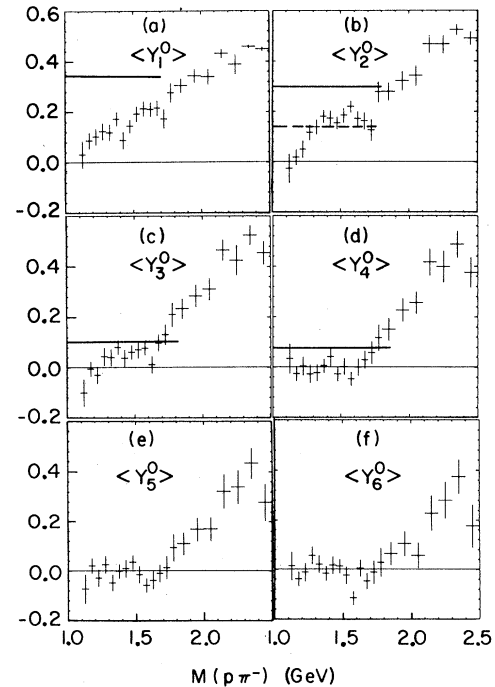
FIG. 9. Values of $\langle Y_l^0 \rangle$ as a function of $M(p\pi^-)$ in the range $0.1 < t' < 0.3$ $(\text{GeV}/c)^2$. The horizontal lines indicate upper limits discussed in the text.
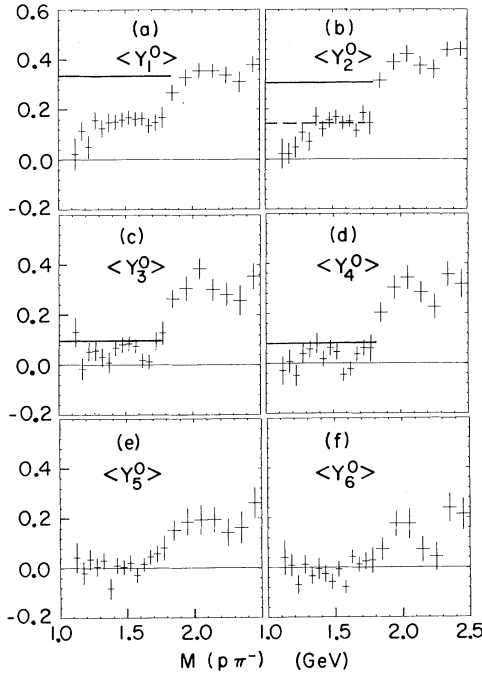
FIG. 10. Values of $\langle Y_l^0 \rangle$ as a function of $M(p\pi^-)$ in the range $t' > 0.3$ $(\text{GeV}/c)^2$. The horizontal lines indicate upper limits discussed in the text.

given in Tables I, II, and III and form the basis of the partial-wave analysis discussed below. The $\langle Y_l^m \rangle$ for $m \neq 0$ are all consistent with zero at all masses and for all regions of momentum transfer.[8]

We observe that the behavior of both $\langle Y_1^0 \rangle$ and $\langle Y_2^0 \rangle$ in the lowest t' interval (see Fig. 8) is significantly different from that seen in the higher t' intervals (see Figs. 9 and 10), particularly in the mass region below 1.7 GeV. This is independent confirmation of the feature already suggested by

Fig. 7 and expressed quantitatively via the two exponentials of Eq. (2) that somewhat different processes are occurring at very low and at higher momentum transfers.

III. PARTIAL-WAVE ANALYSIS

In an attempt to gain a more detailed understanding of the diffractive dissociation we have compared the data of Tables I, II, and III to a simple model involving Pomeranchukon exchange, the Pomeranchukon being considered here as a $J^P = 0^+$ particle. Thus the incident neutron interacts with this simple Pomeranchukon to form a final N^* which decays into $p\pi^-$. This picture is consistent with the experimental observation that $\langle Y_l^m \rangle = 0$ for $m \neq 0$. We have subtracted out the $K^+\Delta^0$ contribution which of course is not accounted for by this model, and all subsequent results incorporate a small correction which takes care of this removal.

We have attempted to interpret the data of Figs. 7 to 10 in the $N\pi$ mass region below 1.7 GeV, in terms of a simple model in which we consider that only P_{11}, D_{13}, and F_{15} amplitudes are present. The justification for these choices is as follows:

(1) The low-t' data show dominance by an isotropic component ($\langle Y_l^0 \rangle \approx 0$ for $l > 0$) at masses below 1.4 GeV. The P_{11} state, which has the same quantum numbers as the nucleon, seems a natural candidate to account for this feature. Furthermore the P_{11} state is the lowest-lying $I = \frac{1}{2}$ N^* established in pion-nucleon phase-shift analysis. It should be noted that P_{11} dominance at low $M(p\pi)$ cannot of itself account for the negative values of $\langle Y_2^0 \rangle$ seen at about 1200 MeV in Fig. 8. Δ^0 production while producing an effect in the right direction is much too weak to account for the observed magnitude of $\langle Y_2^0 \rangle$. Aside from a possible statistical fluctuation,

TABLE I. Populations and moments for $t' < 0.1$ $(\text{GeV}/c)^2$.

ΔM (GeV)	Number of events	$\langle Y_1^0 \rangle$	$\langle Y_2^0 \rangle$	$\langle Y_3^0 \rangle$	$\langle Y_4^0 \rangle$
1.00−1.15	82	0.007 ± 0.03	−0.03 ± 0.03	−0.03 ± 0.03	−0.038 ± 0.027
1.15−1.20	172	−0.02 ± 0.02	−0.07 ± 0.02	0.03 ± 0.02	−0.004 ± 0.02
1.20−1.25	176	0.006 ± 0.02	−0.04 ± 0.02	−0.02 ± 0.02	−0.05 ± 0.02
1.25−1.30	192	−0.019 ± 0.02	0.017 ± 0.02	−0.006 ± 0.02	0.005 ± 0.02
1.30−1.35	184	0.007 ± 0.02	0.034 ± 0.02	−0.012 ± 0.02	−0.045 ± 0.02
1.35−1.40	193	−0.015 ± 0.022	0.061 ± 0.02	0.005 ± 0.02	0.022 ± 0.020
1.40−1.45	138	0.035 ± 0.026	0.069 ± 0.023	0.043 ± 0.022	−0.048 ± 0.022
1.45−1.50	122	0.092 ± 0.028	0.113 ± 0.027	0.031 ± 0.028	0.008 ± 0.028
1.50−1.55	101	0.100 ± 0.037	0.116 ± 0.03	0.012 ± 0.03	0.034 ± 0.028
1.55−1.60	78	0.191 ± 0.03	0.133 ± 0.03	−0.036 ± 0.03	−0.055 ± 0.03
1.60−1.65	64	0.174 ± 0.037	0.162 ± 0.033	−0.015 ± 0.04	−0.049 ± 0.037
1.65−1.70	64	0.192 ± 0.039	0.234 ± 0.036	0.064 ± 0.043	0.065 ± 0.031
1.70−1.75	42	0.24 ± 0.04	0.24 ± 0.05	0.17 ± 0.05	0.11 ± 0.05
1.75−1.80	30	0.15 ± 0.05	0.18 ± 0.06	0.14 ± 0.06	0.173 ± 0.063

TABLE II. Populations and moments for $0.1 < t' < 0.3$ (GeV/c)^2.

ΔM (GeV)	Number of events	$\langle Y_1^0 \rangle$	$\langle Y_2^0 \rangle$	$\langle Y_3^0 \rangle$	$\langle Y_4^0 \rangle$
1.10–1.15	25	0.032 ± 0.054	-0.026 ± 0.057	-0.100 ± 0.054	0.034 ± 0.059
1.15–1.20	76	0.086 ± 0.032	0.018 ± 0.032	-0.006 ± 0.030	-0.026 ± 0.029
1.20–1.25	74	0.103 ± 0.033	0.050 ± 0.034	-0.030 ± 0.034	0.004 ± 0.037
1.25–1.30	85	0.124 ± 0.033	0.116 ± 0.031	0.044 ± 0.035	-0.027 ± 0.036
1.30–1.35	94	0.119 ± 0.033	0.138 ± 0.027	0.040 ± 0.033	-0.023 ± 0.033
1.35–1.40	122	0.173 ± 0.028	0.180 ± 0.026	0.081 ± 0.029	0.005 ± 0.028
1.40–1.45	96	0.088 ± 0.035	0.172 ± 0.031	0.037 ± 0.035	0.041 ± 0.036
1.45–1.50	125	0.144 ± 0.028	0.155 ± 0.025	0.061 ± 0.028	-0.028 ± 0.027
1.50–1.55	94	0.193 ± 0.031	0.185 ± 0.029	0.070 ± 0.033	0.002 ± 0.032
1.55–1.60	104	0.214 ± 0.029	0.219 ± 0.024	0.077 ± 0.027	-0.047 ± 0.028
1.60–1.65	92	0.211 ± 0.029	0.171 ± 0.030	0.011 ± 0.034	-0.000 ± 0.034
1.65–1.70	80	0.216 ± 0.030	0.162 ± 0.034	0.099 ± 0.034	0.029 ± 0.036
1.70–1.75	54	0.174 ± 0.039	0.126 ± 0.043	0.131 ± 0.041	0.058 ± 0.045
1.75–1.80	48	0.277 ± 0.039	0.277 ± 0.041	0.211 ± 0.047	0.117 ± 0.053

we have no explanation of this behavior.

(2) The increasing values of both $\langle Y_1^0 \rangle$ and $\langle Y_2^0 \rangle$ can be economically accounted for by a D_{13} state interfering with the P_{11} amplitude postulated above.

(3) The significant increase of $\langle Y_3^0 \rangle$ and $\langle Y_4^0 \rangle$ near 1.65 GeV suggest the strong onset of higher waves. We have chosen the F_{15} state which like the P_{11} and D_{13} satisfies the Gribov-Morrison rule $P = (-1)^{J-1/2}$ connecting parity and angular momentum for diffractively produced baryons.[9]

In terms of the amplitudes for these three states, which we denote by the symbols P, D, and F we can represent the $p\pi^-$ mass spectrum and the moments $\langle Y_l^0 \rangle$ as follows:

$$\frac{dN}{dM} = |P|^2 + 2|D|^2 + 3|F|^2, \quad (4a)$$

$$\langle Y_1^0 \rangle = \frac{4\,\mathrm{Re}\,P^*D + 7.2\,\mathrm{Re}\,D^*F}{\sqrt{12\pi}(|P|^2 + 2|D|^2 + 3|F|^2)}, \quad (4b)$$

$$\langle Y_2^0 \rangle = \frac{2|D|^2 + 3.43|F|^2 + 6\,\mathrm{Re}\,P^*F}{\sqrt{20\pi}(|P|^2 + 2|D|^2 + 3|F|^2)}, \quad (4c)$$

$$\langle Y_3^0 \rangle = \frac{4.8\,\mathrm{Re}\,D^*F}{\sqrt{28\pi}(|P|^2 + 2|D|^2 + 3|F|^2)}, \quad (4d)$$

$$\langle Y_4^0 \rangle = \frac{2.57|F|^2}{\sqrt{36\pi}(|P|^2 + 2|D|^2 + 3|F|^2)}. \quad (4e)$$

Before taking a more detailed look, we examine some general features of the data in relation to Eqs. (4a)–(4e). First of all, the equations (4b)–(4e) imply well-defined maximum values for the moments $\langle Y_l^0 \rangle$ which are shown as solid lines in Figs. 8 to 10. The dashed line shown in the $\langle Y_2^0 \rangle$

TABLE III. Populations and moments for $t' > 0.3$ (GeV/c)^2.

ΔM (GeV)	Number of events	$\langle Y_1^0 \rangle$	$\langle Y_2^0 \rangle$	$\langle Y_3^0 \rangle$	$\langle Y_4^0 \rangle$
1.10–1.15	21	0.022 ± 0.064	0.022 ± 0.060	0.132 ± 0.058	-0.029 ± 0.057
1.15–1.20	49	0.115 ± 0.039	0.023 ± 0.042	-0.016 ± 0.042	0.008 ± 0.046
1.20–1.25	43	0.051 ± 0.046	0.048 ± 0.042	0.054 ± 0.038	-0.049 ± 0.041
1.25–1.30	69	0.157 ± 0.034	0.107 ± 0.038	0.057 ± 0.039	0.039 ± 0.038
1.30–1.35	69	0.125 ± 0.034	0.071 ± 0.038	0.031 ± 0.036	0.058 ± 0.033
1.35–1.40	74	0.148 ± 0.037	0.170 ± 0.037	0.009 ± 0.040	0.081 ± 0.040
1.40–1.45	93	0.150 ± 0.031	0.120 ± 0.031	0.069 ± 0.031	0.018 ± 0.031
1.45–1.50	107	0.159 ± 0.030	0.156 ± 0.030	0.081 ± 0.030	0.063 ± 0.030
1.50–1.55	120	0.168 ± 0.028	0.167 ± 0.028	0.085 ± 0.030	0.046 ± 0.031
1.55–1.60	103	0.162 ± 0.029	0.145 ± 0.027	0.075 ± 0.027	-0.045 ± 0.027
1.60–1.65	130	0.164 ± 0.026	0.152 ± 0.025	0.017 ± 0.029	-0.022 ± 0.029
1.65–1.70	116	0.135 ± 0.028	0.115 ± 0.029	0.012 ± 0.030	0.037 ± 0.029
1.70–1.75	95	0.148 ± 0.033	0.185 ± 0.031	0.096 ± 0.035	0.062 ± 0.037
1.75–1.80	49	0.168 ± 0.042	0.145 ± 0.045	0.128 ± 0.046	0.061 ± 0.053

moments [Figs. 8(b), 9(b), 10(b)] represents the maximum value when the PF interference term of Eq. (4c) is neglected. As shown by the more detailed analysis to be described below, this term is in general quite small, both because the P and F amplitudes are not simultaneously large and because the phase angle between them is near 90°. Comparison of the data with upper limits shown in Figs. 8–10 indicates that these limits are not exceeded for masses below 1.7 GeV. At higher $M(p\pi)$ values more partial waves are required to fit the observed moments. Furthermore it is evident from the behavior of the $\langle Y_4^0 \rangle$ that the D and F waves play a much larger role for $t' > 0.1$ $(\text{GeV}/c)^2$ (Figs. 9, 10) than for $t' < 0.1$ $(\text{GeV}/c)^2$ (Fig. 8).

These general considerations can be made more quantitative in the following way. From Eqs. (4a), (4c), (4e) we have

$$N(P) + N(D) + N(F) = \sum_i \left(\frac{dN}{dM} \right)_i , \qquad (5a)$$

$$N(D) + 1.1 N(F) = \sqrt{20\pi} \sum_i \left(\frac{dN}{dM} \right)_i \langle Y_2^0 \rangle_i , \qquad (5b)$$

$$N(F) = 1.16 \sqrt{36\pi} \sum_i \left(\frac{dN}{dM} \right)_i \langle Y_4^0 \rangle_i , \qquad (5c)$$

in which $N(P)$, $N(D)$, $N(F)$ are the populations corresponding to the P_{11}, D_{13}, and F_{15} states in the $M(p\pi)$ interval 1.1–1.8 GeV, and where the PF interference term of Eq. (4c) has been neglected in obtaining (5b). Taking the sums on the right-hand side of Eqs. (5a), (5b), and (5c) over all mass bins below 1.8 GeV, one obtains for the three t' intervals previously discussed the numerical values shown in Table IV.[10] The corresponding estimates of $N(P)$, $N(D)$, and $N(F)$ are also given in Table IV as are cross-section estimates. It is important to

note that the separation between P and $D + F$ contributions is much more reliable than the separation between D and F, which depends on the rather imprecise values of $\langle Y_4^0 \rangle$. To emphasize this point we have quoted in Table IV only the sum of $\sigma(D) + \sigma(F)$.

One immediately sees from Table IV the following general features: (a) The P_{11} wave population is virtually all concentrated at $t' < 0.1$ $(\text{GeV}/c)^2$; (b) the D_{13} population is significant in all three momentum transfer bins and accounts for most of the population in the region $0.1 < t' < 0.3$ $(\text{GeV}/c)^2$; (c) finally the F_{15} population is small at the lowest momentum transfers and contributes mostly for $t' > 0.3$ $(\text{GeV}/c)^2$. These features have been obtained without any recourse to the shapes of the mass distributions between 1.1 and 1.8 GeV. Inspection of Fig. 7 shows a shift toward higher masses with increasing t' and hints of structure at 1520 and 1688 MeV in the highest t' bin. This is in good agreement with the observations (a), (b), (c). It is natural to associate the steep exponential in Eq. (2) with the P_{11} amplitude and the more gentle t distribution with the D_{13} and F_{15} amplitudes.

We now consider a somewhat more detailed analysis of the experimental data of Tables I–III in terms of the P_{11}, D_{13}, and F_{15} amplitudes. Looking first at the most peripheral region, $t' < 0.1$ $(\text{GeV}/c)^2$, it is clear from Table I and Fig. 8 that our most significant experimental inputs are the mass population and the values of $\langle Y_1^0 \rangle$ and $\langle Y_2^0 \rangle$. Consequently we have chosen as quantities to be determined by the data the magnitude and phase of the P_{11} amplitude and the magnitude of the D_{13} amplitude in each of the twelve 50-MeV mass bins between 1.1 and 1.7 GeV. We have fixed the D-wave phase as that appropriate to a Breit-Wigner of mass 1520 MeV and width 120 MeV, and have fixed

TABLE IV. Estimates of P_{11}, D_{13}, and F_{15} populations for $M(p\pi) < 1.8$ GeV.

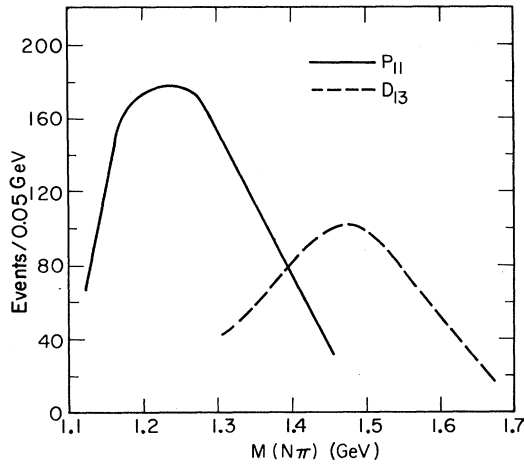|	$t' < 0.1$	$0.1 < t' < 0.3$	$0.3 < t'$ $(\text{GeV}/c)^2$
$\sum_i \left(\frac{dN}{dM} \right)_i$	1610	1147	1112
$\sqrt{20\pi} \sum_i \left(\frac{dN}{dM} \right)_i \langle Y_2^0 \rangle_i$	685 ± 90	1380 ± 90	1190 ± 90
$1.16\sqrt{36\pi} \sum_i \left(\frac{dN}{dM} \right)_i \langle Y_4^0 \rangle_i$	-165 ± 130	27 ± 130	372 ± 130
Estimates from Eq. (5):			
$N(P)$	925	Small	Small
$N(D)$	685	1147	740
$N(F)$	Small	Small	370
Cross-section estimates (μb):			
$\sigma(P)$	58	Small	Small
$\sigma(D) + \sigma(F)$	43	72	70

FIG. 11. Approximate P_{11} and D_{13} contributions to the $M(p\pi^-)$ spectrum for $t' < 0.1$ (GeV/c)^2.

both the mass dependence and the phase of the F_{15} wave to correspond to a Breit-Wigner of mass 1680 MeV and width 130 MeV. The over-all normalization for the F wave was fixed from the event population in the 1.65–1.70-GeV mass bin. Since for $t' < 0.1$ (GeV/c)^2 the F wave is small over almost the whole mass region under consideration, the results for the P and D waves are not particularly sensitive to the above assumptions about the F wave.

The result of this analysis in the region $t' < 0.1$ (GeV/c)^2 is that the data of Table I can be understood in terms of P-wave and D-wave populations whose approximate shapes are shown in Fig. 11. These populations, plus a small F-wave contribution (~80 events), give a reasonable fit provided that the phase of the P wave is chosen to be slowly varying in the interval 105° to 130° between 1.3 and 1.5 GeV.[11] There is no information on this phase below 1.3 GeV because there is no significant D wave to interfere with the P wave. It is very interesting to note that the P_{11} amplitude seen in phase-shift analysis exhibits similar behavior, both in magnitude and phase, as seen here, although in an $N\pi$ mass range shifted 200 MeV higher. Thus whereas our P-wave peak is at about 1250 MeV, the $P_{11}N^*$ (Roper resonance) is quoted to have a mass of about 1470 MeV.[12] Our observed D_{13} amplitude peaks slightly lower than the accepted resonance value of 1520 MeV, but in this case the shift is at most 50 MeV. On the other hand the width of the D state seems somewhat broader than the 120 MeV obtained in phase-shift analysis. Finally, it is worth noting that the P- and D-wave populations determined from the detailed analysis just described integrate to nearly the same values as those quoted in Table IV.

We now consider the higher t' regions portrayed in Figs. 7(b), 7(c), 9, and 10. As already seen in Table IV, the population is dominated by the D and F amplitudes. There is an interesting independent confirmation of this: The rather substantial values of $\langle Y_1^0 \rangle$ and $\langle Y_3^0 \rangle$ observed over most of the mass region 1.1–1.7 GeV are in the ratio $\langle Y_1^0 \rangle / \langle Y_3^0 \rangle \sim 2.3$ expected from Eqs. (4b) and (4d) if only the DF interference contributes to (4b). Unfortunately the only basis for separating the D and F contributions from each other is the values of $\langle Y_4^0 \rangle$, which are not nearly precise enough for this purpose on a bin-by-bin basis. Consequently there is little more that we can say than is already said in Table IV.

IV. DISCUSSION AND CONCLUSIONS

From the data and analysis just discussed, it is seen that the major structure produced at low t in the baryon diffractive dissociation can be interpreted as a P_{11} state whose central mass peak occurs at around 1250 MeV, and whose width is around 300 MeV. Phase-shift analyses of formation experiments show a state of the same quantum numbers and width, $N^*(1470)$, whose central mass is about 200 MeV higher. One now must ask whether in some sense these two states are the same or are different.

If the same P_{11} state is involved in both formation experiments and diffractive dissociation, one must postulate a mechanism which, in the latter process, shifts the resonance to substantially lower mass. That such mechanisms exist is already known from ρ photoproduction, which is also a diffractive process. Thus the photoproduced ρ has a mass spectrum shifted downward by about 20–30 MeV from its usual position.[13] Interpretations of this distortion have been given in terms of (a) multiplicative factors which favor low masses (Ross-Stodolsky model),[14] (b) interference with other diagrams producing background in the same partial wave as the resonance (Söding model).[15]

These mechanisms predict distortions which depend linearly or quadratically on the resonance width. Thus, since the $N^*(1470)$ is very broad ($\Gamma \approx 300$ MeV), it may not be too surprising to find that the shift in the central mass value is much larger than the value observed for the ρ.

To develop a little more understanding of what is actually happening, it is interesting to compare our data with those obtained in missing-mass experiments of the form

$$p + p \to p + N^{*+} , \tag{6a}$$

$$\pi^- + p \to \pi^- + N^{*+} , \tag{6b}$$

where only the outgoing p or π^- are detected and the missing mass of the N^* is inferred by energy

and momentum conservation. Such experiments differ from ours in that not only the $N\pi$ but in fact all decay modes of the N^* are included. Therefore the information derived from the two types of experiment is complementary.

Studies of both reactions (6a) and (6b) at various energies show the production of bumps at 1.24, 1.41, 1.52, 1.69, and 2.19 GeV.[16] Of these, at least the 1.41-, 1.52-, and 1.69-GeV states and perhaps the 2.19-GeV state seem to have cross sections nearly independent of incident energy, and are therefore most probably produced by diffractive dissociation of an incident nucleon. At very low momentum transfers $[|t| < 0.1 \ (\text{GeV}/c)^2]$, the 1.41-GeV state dominates the data; furthermore its momentum transfer dependence, namely $\sim e^{15t}$, is far sharper than that for the higher-mass states, namely $\sim e^{4t}$.

The similarity of the momentum transfer dependence of this 1.41-GeV bump to that of our observed P_{11} state is striking and suggests that they are closely related. However, the central mass values observed in the counter experiments of 1.405 ± 0.015 GeV [reaction (6a)] and 1.412 ± 0.013 GeV [reaction (6b)] are substantially higher than the central value of 1.25 GeV observed in our experiment for the P_{11} state. This difference is necessarily connected with the fact that the counter experiments detect both the elastic $(N\pi)$ and the inelastic $[N\pi\pi, \ \Delta(1236)\pi, \ \text{etc.}]$ final states of the N^*. This implies that either (a) the 1.25- and the 1.41-GeV states from the missing-mass experiments are distinct enhancements, the first decaying via $N\pi$ and the second via inelastic decay modes, produced by nearly identical mechanisms, or (b) that both enhancements arise from the diffractive production of the same resonance, but that dynamical factors, such as those suggested by Ross and Stodolsky, Söding, or others, produce a substantial downward shift in the $N\pi$ mass spectrum relative to the $N\pi\pi$ spectrum. It should be noted that the high threshold for a $\Delta(1236)\pi$ decay mode, namely 1370 MeV, would prevent any comparable shift in that mode.

Hypothesis (a) would require an assumption, as suggested by Morrison,[17] that special types of resonances are produced in diffractive dissociation (D resonances) which are not seen in phase-shift analysis. One can consider as a special case of the D-resonance hypothesis the possibility that the duality arguments of Chew and Pignotti[18] are not valid, and that the 1.25- and 1.41-GeV states are multiperipheral low-mass $N\pi$ and $\Delta(1236)\pi$ enhancements not connected with normal N^* states.

We believe that hypothesis (b) above is more likely to be correct for the following reasons:

(i) There is a low-lying P_{11} state established in phase-shift analysis, the $N^*(1470)$. It seems attractive to relate our P_{11} state and the 1.41-GeV enhancement with that N^*.

(ii) The great similarity in the t distributions for both the P_{11} state in the present experiment and the 1.41-GeV state for the counter experiments makes it natural to assume both states to be the same.

(iii) In the one well-known example of diffractive production of an established resonance, namely ρ^0 photoproduction, the ρ^0 mass spectrum is shifted downward by about 20–30 MeV from its position in other experiments.

It is clearly of interest to study in more detail the relation between the inclusive counter experiments and our exclusive study of reaction (1). This would best be done by investigating all other relevant channels and superposing them to give the inclusive reaction $K^+ n \rightarrow K^+$ (missing mass). This procedure is not possible, particularly in the deuterium reaction. Consequently to obtain a qualitative picture we have used the results of a previous study of the reaction

$$K^+ p \rightarrow K^+ \pi^+ \pi^- p \tag{7}$$

at 9 GeV/c (Ref. 19) and have superposed the $p\pi^-$ spectrum from reaction (1) and $\pi^+\pi^- p$ spectrum from reaction (7) with relative weights calculated in the following fashion. Assuming that for both (1) and (7) the low $M(p\pi^-)$ and $M(p\pi^+\pi^-)$ populations are dominated by baryon states of isospin-$\frac{1}{2}$ produced by diffractive dissociation and that the nucleon–two-pion system consists principally of $\Delta\pi$, we have multiplied the cross sections by Clebsch-Gordan factors of $\frac{3}{2}$ and $\frac{9}{5}$ for $p\pi^-$ and $p\pi^+\pi^-$, respectively, to take approximate account of undetected channels.[20] The total baryon mass spectra, for single-pion-plus-double-pion production, are shown in Fig. 12 for the t' ranges discussed earlier.

Qualitatively, the mass spectra of Fig. 12 are quite similar to those obtained in the counter missing-mass experiments in the same momentum transfer regions.[21] In particular, for $t' < 0.1$ (GeV/$c)^2$ the large bump at 1.45 GeV in Fig. 12 is the structure which, in the counter experiments, is interpreted in terms of the production of $N^*(1.41)$ and $N^*(1.52)$. In this low-t' region the structure in the single pion production does *not* follow the shape of the total mass spectrum but is shifted downward by about 150–200 MeV. Indeed, one can easily show that the amount of the P_{11} $p\pi^-$ contribution in the 1.4–1.5-GeV region of $M(p\pi^-)$ is far smaller than would be expected by taking the total apparent $N^*(1.41)$ contribution and multiplying it by the elasticity of the Roper resonance determined by phase-shift analysis, which is 0.6.[12] The total P_{11} contribution in reaction (1) is roughly
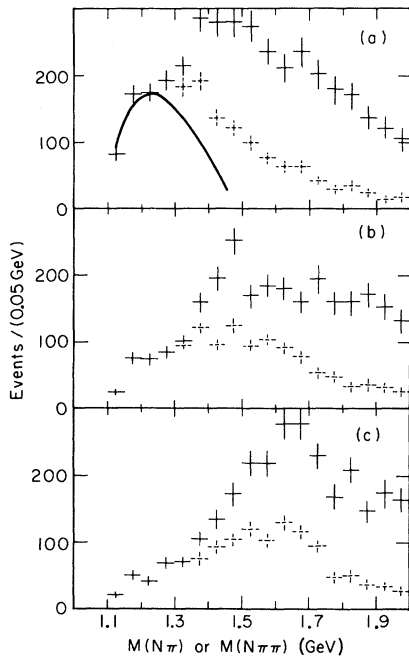
FIG. 12. $M(N\pi)$ and $M(N\pi\pi)$ spectra for the t' regions (a) $t' < 0.1$ (GeV/c)^2, (b) $0.1 < t' < 0.3$ (GeV/c)^2, (c) $t' > 0.3$ (GeV/c)^2. The solid crosses show $M(N\pi) + M(N\pi\pi)$, the dashed crosses show $M(N\pi)$, and the solid curve is the P_{11} contribution to the $M(N\pi)$ spectrum.

right from this point of view, but it simply comes at a very low mass, namely 1.25 GeV.

If our interpretation of the P_{11} enhancement in terms of a shifted Roper resonance is correct we have a remarkable illustration of duality, as applied by Chew and Pignotti. Indeed the t-channel multiperipheral interpretation leads in a natural way to differently located mass peaks for the $N\pi$ and $\Delta(1236)\pi$ final states just in consequence of the different thresholds. On the other hand, if as suggested here both peaks represent the same resonance, consistency of the two types of interpretation as required by duality demands a dynamical mechanism which shifts the $N\pi$ decay mode down-

ward relative to the $\Delta\pi$ mode.

We now come back briefly to the dynamical factors which may be shifting our observed P_{11} mass spectrum to a peak as low as 1.25 GeV. As pointed out in the analysis of the previous section, there is not only a mass shift but a shift of phase as well, that is, at 1250 MeV the phase of the P_{11} state is about the same as the phase observed in the analysis of formation experiments at about 1450 MeV. This shift of phase is not easily accounted for by either the Ross-Stodolsky or the Söding models. Thus this distortion remains a challenge for theory unresolved by present models. Although we have stressed the P_{11}, there is no reason to assume that distortions are absent from the other states such as the D_{13} and the F_{15}. Because of their relatively narrow widths, the distortions will be far smaller, and it is therefore not surprising that we cannot establish them unambiguously.

We conclude with a brief comment on the impact of these results on the analysis of boson diffractive dissociation into the A_1 and Q enhancements. If one accepts the very suggestive relationship between the diffractively produced P_{11} state and the $N^*(1470)$ resonance observed in formation experiments, it seems likely by analogy that the A_1 and Q are also resonant states or groups of resonant states. A detailed understanding of the structure of the A_1 and Q must await a more complete understanding of the dynamical effects which distort the diffractive mass spectra.

ACKNOWLEDGMENTS

---

*Present address: Department of Physics, Tel-Aviv University, Tel-Aviv, Israel.

†Work supported by the U. S. Atomic Energy Commission.

‡Present address: Department of Physics, California Institute of Technology, Pasadena, Calif. 91109.

§Present address: Groupe GAP, Department Saturne, C.E.N.S., Essonnes, France.

‖ On sabbatical leave from University of California, Berkeley; Guggenheim Fellow at CERN (1972).

[1]A. Firestone *et al.*, Phys. Rev. D **5**, 505 (1972).

[2]The given cross section measures the rate for the reaction $K^+ d \rightarrow K^+ \pi^- p p$ in which one or both of the out-

going protons have momenta less than 300 MeV/c. Without the 300-MeV/c cutoff, the cross section is 420 ± 20 μb; this figure is probably a closer approximation of the value for the reaction $K^+ n \rightarrow K^+ \pi^- p$.

[3]A. Firestone *et al.*, Phys. Letters **36B**, 513 (1971); Phys. Rev. D **5**, 2188 (1972); Phys. Rev. Letters **26**, 1460 (1971).

[4]K. Boesebeck *et al.*, Nucl. Phys. **B28**, 381 (1971).

[5]G. Yekutieli *et al.*, Nucl. Phys. **B40**, 77 (1972).

[6]M. J. Longo *et al.*, Phys. Letters **36B**, 560 (1971).

[7]J. C. Berlinghieri *et al.*, Nucl. Phys. **B8**, 333 (1968); V. G. Lind *et al.*, *ibid.* **B14**, 1 (1969).

[8]It is worth noting that, while the mass spectra are

similar, the moments $\langle Y_l^m \rangle$ seem to differ significantly from those observed by Yekutieli *et al.* (Ref. 5) in the reaction $pn \rightarrow pp\pi^-$. Indeed Yekutieli *et al.* do observe nonzero values of Re$\langle Y_l^m \rangle$ with $m \neq 0$. Our $p\pi^-$ decay angular distributions also seem to differ from those observed in diffractive dissociation from a carbon target (Ref. 6).

[9]V. N. Gribov, Yad. Fiz. <u>5</u>, 197 (1967); D. R. O. Morrison, Phys. Rev. <u>165</u>, 1699 (1968).

[10]As indicated earlier, comparison of the upper limits for $\langle Y_l^0 \rangle$ based on Eqs. (4) with the data of Figs. 8–10 shows no contradiction below 1.7 GeV. We have slightly stretched this limit of applicability to 1.8 GeV in deriving the results of Table IV in an attempt to include the total contribution of the F_{15} state, whose resonance central value is about 1.69 GeV.

[11]The P_{11} phase is determined from the *PD* interference term and from the choice of the D_{13} phase as that phase which corresponds to a Breit-Wigner shape of mass 1520 MeV and width 120 MeV; that is, $\phi = \tan^{-1} \{\Gamma/2[M_0 - M(p\pi)]\}$, where $\Gamma = 120$ MeV and $M_0 = 1.52$ GeV.

[12]Particle Data Group, Rev. Mod. Phys. <u>43</u>, S1 (1971), see p. 51.

[13]See, for example, J. Ballam *et al.*, Phys. Rev. D <u>5</u>, 545 (1972).

[14]M. Ross and L. Stodolsky, Phys. Rev. <u>149</u>, 1172 (1966).

[15]P. Söding, Phys. Letters <u>19</u>, 702 (1965).

[16]G. Cocconi *et al.*, Phys. Letters <u>8</u>, 134 (1964); E. W. Anderson *et al.*, Phys. Rev. Letters <u>16</u>, 855 (1966); I. M. Blair *et al.*, *ibid.* <u>17</u>, 789 (1966); C. M. Ankenbrandt *et al.*, Phys. Rev. <u>170</u>, 1223 (1968); E. W. Anderson *et al.*, Phys. Rev. Letters <u>25</u>, 699 (1970); W. E. Ellis *et al.*, *ibid.* <u>27</u>, 442 (1971); and R. M. Edelstein *et al.*, Phys. Rev. D <u>5</u>, 1073 (1972).

[17]D. R. O. Morrison, Rapporteur report in *Proceedings of the Fifteenth International Conference on High-Energy Physics, Kiev, U.S.S.R., 1970* (Atomizdat, Moscow, 1971).

[18]G. F. Chew and A. Pignotti, Phys. Rev. Letters <u>20</u>, 1078 (1968).

[19]C. Fu *et al.*, Nucl. Phys. <u>B18</u>, 93 (1970).

[20]For purposes of relative normalization of reactions (1) and (7), we have taken for the cross section of (7) its value at 12 GeV/c, namely 935 ± 30 μb, as measured by P. J. Davis *et al.*, Phys. Rev. D <u>5</u>, 2688 (1972).

[21]The ordinates of Fig. 12 can be converted to approximate cross sections in μb by division by 10. These cross sections are roughly 30% smaller than those for $\pi^- p$ at 12 GeV/c (Ref. 16). This is reasonable in view of the fact that K^+N cross sections are typically somewhat smaller than πN cross sections.